# Geometric Configuration Constraints for Large Deep Space Network Arrays

D. L. Jones[1]

*The problem of selecting the relative positions of antennas in a large radio array has many degrees of freedom. This article considers ways to constrain this problem and arrive at geometric configurations that optimize array performance parameters of relevance to spacecraft tracking applications. A comparison with configurations developed for radio astronomy arrays illustrates the differences between the constraints that apply to spacecraft tracking and to aperture synthesis radio imaging. Despite these differences, many of the techniques and tools used in the design of radio astronomy array configurations are also applicable to Deep Space Network (DSN) array configurations.*

## I. Introduction

One approach to obtaining much higher data rates from future deep-space missions is to increase the signal-collecting aperture on the ground. Large arrays composed of numerous small, mass-produced radio antennas promise to provide a significant reduction in cost per unit of collecting area compared to current large antennas. Consequently, large arrays are being developed for future Deep Space Network (DSN) use.

One of the many issues involved in the design of a radio array is the distribution of individual antenna locations—the geometric configuration of the array. The array configuration is a free design parameter that can have a strong effect on the array performance.

## II. Design Requirements for DSN Array Configurations

Geometric configurations (antenna positions) for a DSN array must satisfy several criteria:

[1] Tracking Systems and Applications Section.

The research described in this publication was carried out by the Jet Propulsion Laboratory, California Institute of Technology, under a contract with the National Aeronautics and Space Administration.

(1) The configuration should be compact, which allows accurate correction of phase errors caused by variations in tropospheric water vapor. These variations have a typical scale length of a few hundred meters, so antennas separated by less than this will see correlated phase changes, and the amplitude of differential phase changes will be reduced. This is particularly important at 32 GHz (Ka-band), since the magnitude of atmospheric phase errors on a given baseline will scale with frequency.

(2) The configuration must be sufficiently extended to avoid unacceptable levels of antenna shadowing at low elevations. This sets a minimum baseline length that a large fraction of the total number of baselines must exceed.

(3) The total extent of an array cluster must fit within the (accessible, relatively flat) available land.

(4) The configuration should produce an instantaneous synthesized beam with low side-lobe levels (especially in directions near the ecliptic). This minimizes the noise contribution from nearby planets, the Sun, or other spacecraft, and also allows separate array beams to track multiple spacecraft simultaneously even on nearly identical frequencies.

(5) The configuration should allow flexibility in defining and changing sub-arrays.

(6) The configuration should be scalable. Beginning with only a few antennas, a series of good configurations should be produced as additional antennas are added to the array.

These criteria differ from those traditionally applied to the design of arrays for radio astronomy.

## III. Radio Astronomy Array Configurations

It is useful to consider how radio astronomy array configurations are determined, because the astronomy community has a long history of designing and using arrays with large numbers of antennas. Although aperture synthesis imaging is the primary goal of most radio astronomy arrays, and this is not a requirement for spacecraft tracking, many of the techniques and software tools developed for optimizing array configurations can be applied to goals other than imaging. Thus, they are relevant for the study of DSN array configurations.

The configurations used for arrays in radio astronomy have undergone a significant evolution during the past several years. General purpose arrays designed and built prior to the year 2000 had relatively small numbers of antennas (30 for the Giant Metrewave Radio Telescope, 27 for the Very Large Array, and fewer for the Westerbork Synthesis Radio Telescope, Ryle Telescope, Very Long Baseline Array, and the Australia Telescope Compact Array). As a result, they have had to rely on Earth rotation aperture synthesis to produce high-quality radio images. Each interferometer baseline samples one point of the two-dimensional visibility function (the Fourier transform of the sky brightness distribution) at a given time, but the projected baseline changes as the Earth rotates, and so the visibility function can eventually be sampled at many points. The configurations of existing arrays were designed to produce good sampling of the visibility function (or the $u, v$ plane, the plane onto which baselines are projected for a given source direction) during tracks of many hours duration.

The Allen Telescope Array (ATA) represents a dramatic change in philosophy. For the first time, the number of antennas (350) is sufficiently large that there is no need to rely on Earth rotation synthesis to obtain very dense sampling of the visibility or $u, v$ plane. A configuration optimized to give a nearly Gaussian beam profile was developed by Bock [1] using Boone's technique [2] for interactively approaching a predetermined distribution of $u, v$ samples. The resulting ATA configuration is shown in Fig. 1.

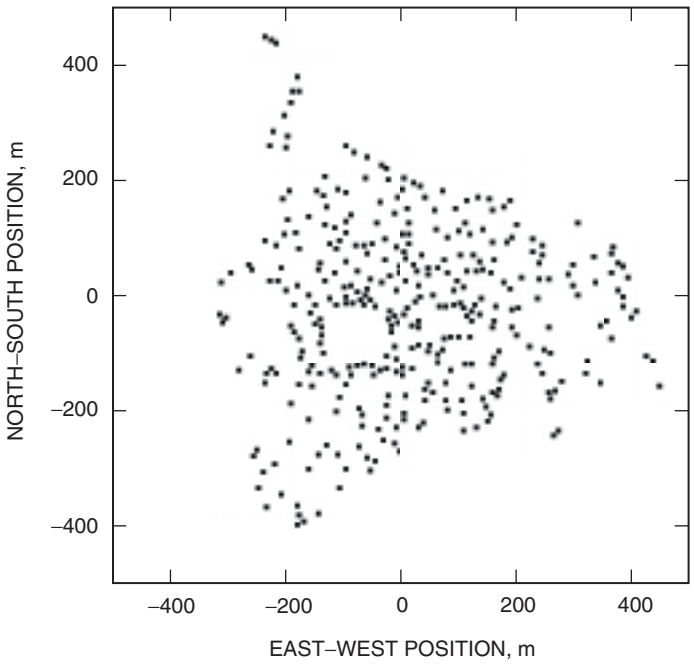


**Fig. 1. Final geometric configuration of the 350-antenna Allen Telescope Array, optimized for a Gaussian synthesized beam shape over a wide range of declinations under constraints imposed by existing buildings, roads, and small-scale topography at the site in Hat Creek, California.**

The somewhat odd look of this configuration is required to avoid existing buildings, roads, and lava flows. Despite these constraints, the configuration in Fig. 1 produces a very high quality snapshot beam. This indicates that for arrays containing hundreds of antennas there are a large number of possible configurations that provide nearly identical synthesized beams.

Recently, the Atacama Large Millimeter Array (ALMA) has been approved for construction with 64 antennas. However, even in this case, the configuration is based on long tracks and periodic transport of antennas between a large number of possible locations to produce good $u, v$ coverage. The configuration studies done for ALMA have produced a number of innovative and powerful algorithms to define and optimize array configurations under various assumptions about the desired result. Some of the approaches taken for ALMA configurations include circular arrays [16,17,19], logarithmic spirals [6,7], uniform $u, v$ coverage [9], convergence to more general $u, v$ density distributions [2–4], and minimization of near-in side lobes [10]. Many of these approaches are relevant for the design of arrays other than ALMA, including DSN arrays.

A unique approach has been developed for the Low Frequency Array (LOFAR), whose configuration both within individual clusters and for the over-all array follows a fractal geometry with an exponential scaling law [5]. This configuration has a great deal of flexibility in terms of imaging performance, but is possible only because of the extremely large number of antenna elements (approximately 13,000) in the LOFAR design.

The Square Kilometer Array (SKA) is the most ambitious radio array currently planned, and a large amount of effort has been devoted to studies of suitable configurations. The majority of these have concentrated on logarithmic spiral configurations because of their ability to provide well-defined synthesized beams over a wide range of angular resolutions. As a result, SKA configurations are unlikely to be directly relevant for spacecraft tracking arrays.

The goal of most future radio astronomy array configuration studies is to produce $u, v$ sampling with a truncated Gaussian density distribution, and thus synthesized beams with a nearly Gaussian profile. This is good for high dynamic range imaging, but it implies a low-density region of "outlier" antennas that could be difficult to keep phased properly in marginal weather conditions. Unlike most radio astronomy observations, spacecraft tracking cannot wait for improved weather. Very reliable and robust array phasing will be essential if we are to maintain a high level of array availability for spacecraft links.

## IV. DSN Array Configuration Design

Preliminary results of DSN array configuration studies are given in [8]. This article updates the earlier work to include sequences of arrays over a larger range of antenna number and detailed antenna shadowing calculations.

The procedure used was to set a value for $N$, the total number of antennas; the maximum extent of the array (the diameter of the area within which all the antennas are located); and a minimum allowed separation between any pair of antennas. A configuration optimization program for radio arrays written by L. Kogan at the National Radio Astronomy Observatory (NRAO) was used to minimize the side lobes within the area of the antenna primary beams [10]. The algorithm used was developed to help the design of astronomical radio arrays, but it is pertinent to DSN array design because the level of nearby side lobes determines the extent to which separate spacecraft using the same frequencies can be tracked simultaneously within the primary beam area. Side-lobe levels also determine the sensitivity of the array to interference pickup from different directions and to emission from a planet or other objects close to a target spacecraft.

An analytic expression for the derivative of the synthesized array beam side-lobe levels with respect to a given shift in antenna location was used to calculate an improved configuration by shifting all antenna locations by distances and directions determined by the derivative values. This is an iterative algorithm that requires a rapidly increasing amount of computing time as $N$ increases. Constraints on allowed antenna locations (due to site topology, for example) can be imposed, but were not used in the studies reported here. These can be added when a precise location for the array cluster is chosen.

Negative side-lobe levels for an $N$-antenna array are $1/(N-1)$, independent of the configuration [11,12]. The peak amplitude of positive side lobes, however, does depend on the array configuration as well as on $N$. For large-$N$ arrays, the positive side lobes generally will be larger than the negative side lobes (in absolute value). The algorithm of Kogan [10] moves the larger side lobes outside of the primary antenna beam area. The amplitude of synthesized beam side lobes outside the primary beam area is unimportant because the primary beam response will suppress any unwanted emission from those directions.

## V. Results

Configuration requirements based on the criteria listed in Section II and consistent with potential sites available at Goldstone can be summarized as

(1) Maximum diameter of the area occupied by the cluster of antennas: 1 km

(2) Minimum separation between any pair of antennas: 30 m

(3) Maximum loss due to antenna shadowing at 10-deg elevation: 1.5 dB

(4) Maximum loss due to antenna shadowing at 20-deg elevation: 0.5 dB

(5) Maximum side lobe within the primary beam area at transit: $1/N$

(6) Minimum number of antennas for good performance: 25

(7) Maximum number of antennas (within a 1-km-diameter area): 500

Initially, a 25-antenna configuration was developed that in turn was held fixed as the core of a 100-antenna configuration. Similarly, the 100-antenna solution was held fixed while an additional 300 antenna locations were optimized to produce a 400-antenna configuration. This generates a series of configurations that can be produced by simply adding more antennas to the previous configuration and thus represents a logical construction sequence.

For initial construction, a 12-antenna configuration also was created by selecting an appropriate subset of antenna locations from the optimized 25-antenna configuration. The locations of the 12 antennas were not separately optimized because with so few antennas the instantaneous synthesized beam will have relatively high side lobes independent of the exact configuration. The initial 12 antenna locations do cover almost the same physical area as the optimized 25-antenna array, so early observations of phase stability will be directly applicable to the next stage of construction.

Figure 2 shows the 12-, 25-, 100-, and 400-antenna configurations.

The instantaneous synthesized beam produced by the 400-antenna configuration in Fig. 2 at zenith and at a declination of 0 degrees is shown in Figs. 3(a) and 3(b), respectively. Note that the region within the primary antenna beam area is nearly devoid of side-lobe peaks at the 1 percent level in both cases. More distant side lobes will be suppressed by the primary beam and thus will not contribute to stray radiation or radio frequency interference (RFI) pickup. The root-mean-square (rms) side-lobe level within the primary beam area is less than 0.3 percent, indicating that multiple spacecraft could be tracked at the same frequency simultaneously by this array with at least 25 dB of isolation between the signals. (This assumes the spacecraft are all within the primary beam area but separated by more than the synthesized beam width of about 1 arcsecond or 5 microradians. Spacecraft within the synthesized beam also could be tracked simultaneously if they differed in frequency or polarization.)

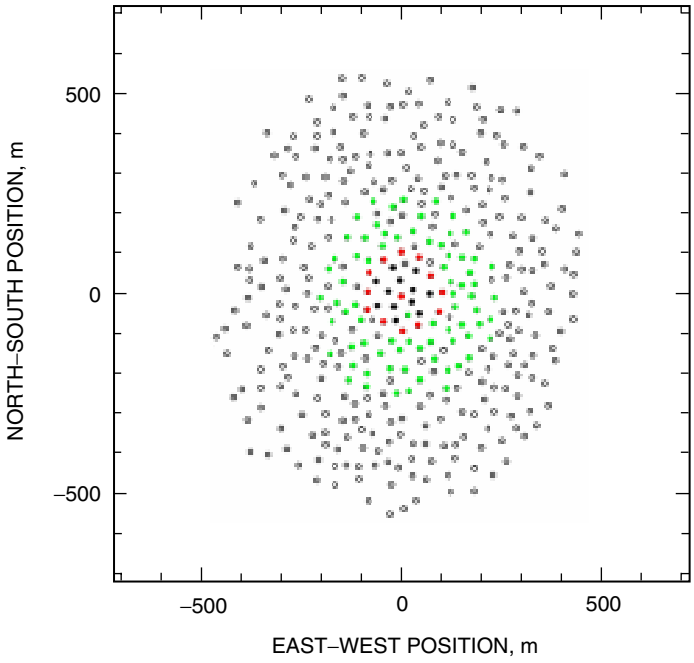


**Fig. 2. The proposed 400-antenna configuration, with subsets shown in color: 12-antenna array (black), 25-antenna array (black plus red), and 100-antenna array (black plus red plus green).**

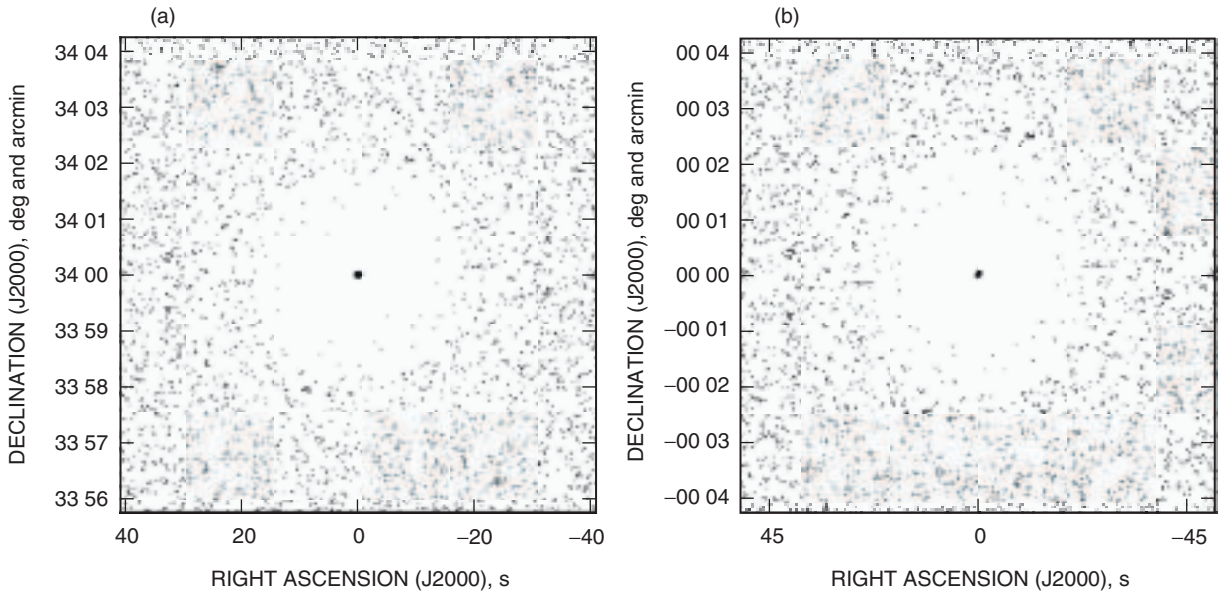


**Fig. 3. Instantaneous synthesized array beams at transit for declinations of (a) 34 deg north and (b) 0 deg. These beams are for observations at Ka-band and assume equal amplitude weighting of all antennas for maximum sensitivity to point sources such as spacecraft. The lowest contours plotted are ±1 percent of the synthesized beam peak. The primary beam width (full width at half maximum) for a 12-m antenna at 32 GHz is approximately 3 arcmin. Levels are –10, –5, –2, –1, 1, 2, 5, 10, 15, 25, 35, 50, 70, and 95 percent.**

It is worth noting that the 5-microradian synthesized beam width implies that plane-of-sky position measurements can be made with an accuracy of about 5000/(SNR) nanoradians. For high signal-to-noise ratio (SNR) signals, this accuracy may be useful for real-time navigation, even though it is far lower than the accuracy available using very long baseline interferometry (VLBI) techniques, because it will be available continuously and nearly instantaneously. For example, the position of a signal with SNR = 100 could be determined to within 50 nanoradians or 10 milliarcseconds.

For compact configurations of the sort shown in Fig. 2, antenna shadowing at low elevations is always a concern. Figure 4 shows the fraction of the total array aperture that is shadowed at elevations of 20, 15, and 10 degrees for the 400-antenna configuration shown in Fig. 2. The shadowing is shown as a function of azimuth angle. It is assumed that data from any partially shadowed antenna will be lost, so the fraction of the array shadowed is equal to the fraction of antennas shadowed. This conservative assumption is based on the possibility that mutual coupling between shadowed antennas may introduce spurious coherent signals that will be difficult to excise during signal processing.

The average amount of shadowing at 20, 15, and 10 degrees is about 7, 14, and 27 percent, respectively. This corresponds to effective gain losses of about 0.3, 0.7, and 1.4 dB. For comparison, the 70-m DSN antenna gain curves for 8.4 GHz (X-band) show losses of up to 0.4 dB at an elevation of 20 degrees, 0.5 dB at 15 degrees, and 0.75 dB at 10 degrees [14]. Except at the lowest elevation, these are quite similar to the losses due to shadowing for the array. At Ka-band, the low-elevation gain losses of large DSN antennas are expected to be significantly larger than the array losses due to shadowing. The small-diameter antennas of the array are very stiff and are expected to have nearly flat gain curves even at Ka-band.

In fact, the assumption that data from partially shadowed antennas will not be used is probably too conservative. Studies of shadowing done at the Australia Telescope Compact Array indicate that the dominant source of extraneous signals picked up by a shadowed antenna is not reflection off of antenna structural elements or radiation diffracted around the rim of the shadowing reflector, but coherent

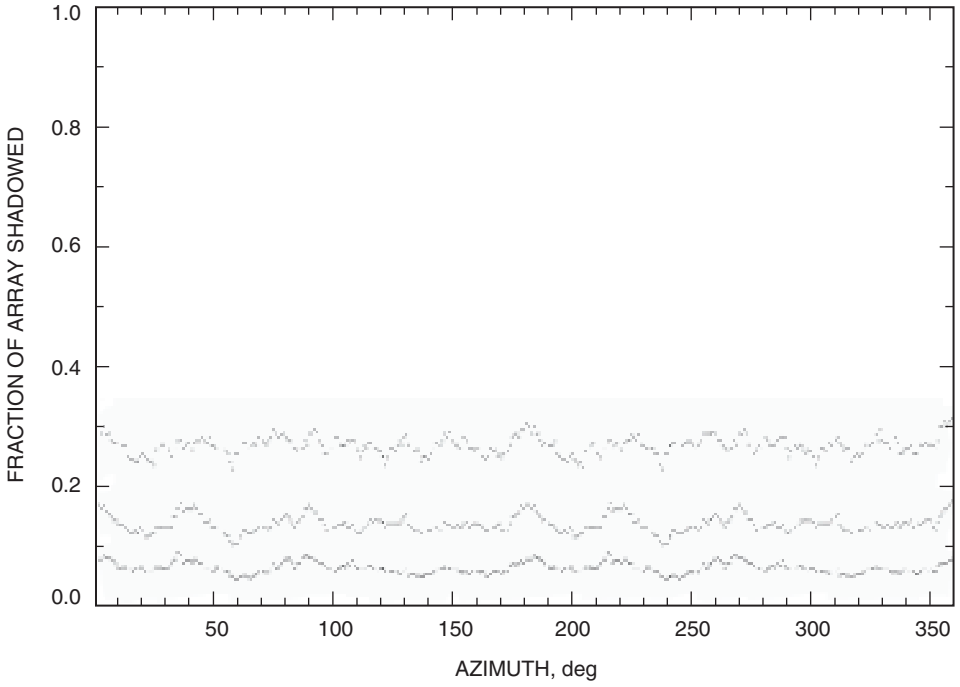


**Fig. 4. Fraction of the array collecting area affected by antenna shadowing as a function of azimuth. The three curves are for elevations of 10 deg (top), 15 deg (middle), and 20 deg (bottom).**

radiation from gaps between the main reflector panels of the shadowing antenna [15]. For antennas with a one-piece main reflector, such as hydroformed antennas, this source of mutual coupling will not exist. Consequently, it is quite possible that we will be able to use data from partially shadowed antennas by allowing for any shift in effective phase center along with the reduction in effective collecting area. In that case, the array gain loss due to shadowing will be less than shown in Fig. 4. The inevitable distortion of the primary beam of a partially shadowed antenna will have little effect on performance near the field-of-view center.

How critical is the location of any particular antenna in an array of 100 or more antennas? Bock [1] finds that random antenna position changes of 1 to 2 meters rms have a negligible effect on performance for the ATA (350 antennas within a diameter of about 1 km). This suggests that we can relocate antennas from their optimal positions to avoid small-scale terrain problems without causing significant performance degradation. In any case, the actual antenna positions will be determined to a fraction of a wavelength at Ka-band by observing a set of radio sources with well-known sky positions (see, for example, [18]).

## VI. Conclusions

The motivation for developing arrays of many small, inexpensive antennas for spacecraft tracking is to provide a large increase in sensitivity compared to the current DSN. To achieve this goal reliably, it is essential that correct phasing of the array antennas be maintained over a wide range of observing conditions. This is turn provides a constraint on the size and density of individual array clusters, because atmospheric phase fluctuations increase with increasing antenna separation. Self-calibration techniques (e.g., [13]) can correct for atmospheric phase errors using a spacecraft or celestial radio source signal, but only when an SNR greater than unity can be obtained on time scales shorter than the coherence time imposed by the atmosphere. For shorter baselines, the coherence time is longer, and, consequently, phase calibration will be possible under less stable atmospheric conditions or with weaker signals.

A compromise must be found between minimizing atmospheric phase errors and minimizing antenna shadowing at low elevations. This article presents a series of array configurations that represent reasonable compromises between the two opposing constraints of robust phasing and minimal shadowing. Future work could include studies of how to optimize the distribution of antennas between multiple subarrays, and configurations of multiple, widely separated array clusters to optimize angular navigation measurements.

## Acknowledgments

I thank D. Bagri and R. Preston for helpful discussions and L. Kogan for developing the optimization algorithm used in this work. This work made use of the Astronomical Image Processing System (AIPS), which is distributed by the National Radio Astronomy Observatory.

## References

[1] D. Bock, "The Antenna Configuration of the Allen Telescope Array," ATA Memo 50, University of California, Berkeley, 2003.

[2] F. Boone, "Interferometric Array Design: Optimizing the Locations of the Antenna Pads," *Astron. and Astrophys.*, vol. 377, pp. 368–376, 2001.

[3] F. Boone, "Interferometric Array Design: Distributions of Fourier Samples for Imaging," *Astron. and Astrophys.*, vol. 386, pp. 1160–1171, 2002.

[4] F. Boone, "A Proposal of Optimized Configurations for the ALMA," ALMA Memo 400, National Radio Astronomy Observatory, 2002.

[5] J. D. Bregman, "Concept Design for a Low Frequency Array," *Proc. SPIE*, vol. 4015, pp. 19–32, 2000.

[6] J. Conway, "Self-Similar Spiral Geometries for the LSA/MMA," MMA Memo 216, National Radio Astronomy Observatory, 1998.

[7] J. Conway, "First Simulations of Imaging Performance of a Spiral Zoom Array: Comparisons with a Single Ring Array," ALMA Memo 219, National Radio Astronomy Observatory, 2000.

[8] D. L. Jones, "Geometric Configurations for Large Spacecraft-Tracking Arrays," 2003 IEEE Aerospace Conference, IEEE, paper 03.0203 in proceedings CD, 2003.

[9] E. Keto, "The Shapes of Cross-Correlation Interferometers," *Astrophys. Journal*, vol. 475, pp. 843–852, 1997.

[10] L. Kogan, "Optimization of an Array Configuration Minimizing Side Lobes," MMA Memo 171, National Radio Astronomy Observatory, 1997.

[11] L. Kogan, "Level of Negative Side Lobes in an Array Beam," MMA Memo 218, National Radio Astronomy Observatory, 1998.

[12] L. Kogan, "Level of Negative Sidelobes in an Array Beam," *Publ. Astron. Soc. Pacific*, vol. 111, pp. 510–511, 1999.

[13] T. J. Pearson and A. C. S. Readhead, "Image Formation by Self-Calibration in Radio Astronomy," *Annual Reviews of Astronomy and Astrophysics*, vol. 22, pp. 97–130, 1984.

[14] P. H. Richter and S. D. Slobin, "DSN 70-Meter Antenna X- and S-Band Calibration Part I: Gain Measurements," *The Telecommunications and Data Acquisition Progress Report 42-97, January–March 1989*, Jet Propulsion Laboratory, Pasadena, California, pp. 314–351, May 15, 1989.
http://tmo.jpl.nasa.gov/tmo/progress_report/42-97/97GG.PDF

[15] R. Subrahmanyan and A. A. Deshpande, "Contaminants in ATCA Baselines with Shadowing: A Case Study of Cross Talk in Short-Spacing Interferometers," *M.N.R.A.S.*, in press (astro-ph/0401280), 2004.

[16] D. Woody, "ALMA Configurations with Complete UV Coverage," ALMA Memo 270, National Radio Astronomy Observatory, 1999.

[17] D. Woody, "Radio Interferometer Array Point Spread Functions I. Theory and Statistics," ALMA Memo 389, National Radio Astronomy Observatory, 2001.

[18] M. Wright, "Antenna Position Calibration," ALMA Memo 427, National Radio Astronomy Observatory, 2002.

[19] M. S. Yun and L. Kogan, "Strawperson Donut/Doubling-Ring Configurations," ALMA Memo 320, National Radio Astronomy Observatory, 2000.